Jurnal Polimesin
Department of Mechanical Engineering
State Polytechnic of Lhokseumawe
http://e-jurnal.pnl.ac.id/polimesin

e-ISSN : 2549-1999 No. : 4 Month : August
p-ISSN : 1693-5462 Volume : 21 Year : 2023

Article Processing Dates: Received on 2023-05-26, Reviewed on 2023-05-26, Revised on 2023-07-07, Accepted on 2023-08-16 and Available online on 2023-08-28

Optimization and Design Analysis of 2-kW induction motor shaft by using Finite Element Analysis

Lambert Hotma*, Nur Cholis Majid, Marsalyna, Fandy Septian Nugroho, Achmad Ridho Mubarak, Freddy Marpaung
Research Center of Process and Manufacture Technology Industry, National Research and Innovation Agency South Tangerang, 15314, Indonesia
*Corresponding author**:** lamb004@brin.go.id

Abstract

The shaft is a very critical part of a 2-kW induction motor due to its function to support other vital components, such as the rotor, bearing, and casing. Finite Element Analysis (FEA) is used to analyze the shaft model. A meshing convergence test was conducted prior to the optimization. In which a mesh size of 0.5 mm and a tetrahedron shape are selected for the whole simulation to determine critical areas on the electric motor shaft (EMS). In this study, shaft optimization was conducted by using three manners in a sequential process, namely reducing the shaft seat for the rear bearing, modifying the step in front of the rear bearing, and then making the taper from the step in the previous process. This design modification was made to reduce the shaft mass and the maximum equivalent stress. At first optimization, namely replacing the rear bearing and its mount on the shaft, it succeeded in reducing the axle weight by 2,81%. However, the max equivalent stress increased from 30.347 MPa to 54.756 MPa which is located at the intersection of the stepped area, as well as deformation also increased from 0.002434 mm to 0.0026894 mm at the middle shaft. This drawback is overcome by changing the depth of the stepped area and creating a taper. In which the shaft mass can be reduced from 431.07 g to 408.20 g, as well as max equivalent stress is reduced from 54.756 MPa to 28.637 MPa.

Keywords:
FEA, optimization, shaft, electric motorcycle, weight

1 Introduction

The shaft is one of the crucial components in an electric motor which is used to support other components such as the rotor, bearing, and motor casing. The Shaft is commonly subjected to various loads such as bending, torsion, and shear moment. These loads can induce high stress in an electric motor shaft which may cause material failure [1].

There are two parameters that need to be considered when designing a shaft, namely dimension and material selection. The shaft dimension is basically controlled by the weight of the rotor and bearing type. While the material types should have adequate strength and toughness to endure material failure while receiving static or dynamic load [2].

To acquire a high-quality electric motor shaft (EMS), it is important to gain a proper design of the EMS and perform a series of virtual tests using Finite Element Analysis (FEA). FEA is used to understand failure mechanisms and to find weak spots, areas of stress, and deformation. Besides that, the FEA can be used to optimize the model weight as well as to identify optimal material selection.

FEA is a calculation solution method by dividing the model into tiny elements, such as triangle, square, tetrahedral, and hexahedral, and then the created elements are calculated by using numerical mathematic techniques [3]. These methods have been commonly used to validate the design process because of their capability of solving complex models compared to a modest mathematical analysis method. Moreover, FEA is widely used to simulate numerous processes because of its ability to minimize trial-and-error experiments so that time and resources are saved. [4-5].

Some studies related to FEA have been conducted to optimize the shaft quality. For example, composite derived from carbon fiber can reduce the weight of the propeller shaft [6-7] as well as better angle twist in comparison to the steel material [8]. Another material, namely Ti6Al4V is promising to be used as a material shaft, in which the Ti6Al4V has similar computational results in terms of mechanical properties when compared with SM45C [9].

Design modification for shaft fillet was also investigated to obtain a high-quality shaft. Ali et al developed shaft reinforcement by adding three fillets to reduce stress concentration, marked by R1, R2, and r, depicted in Fig. 1. The shaft reinforcement showed decreased stress of 10.38% and better performance in all variations made [10].

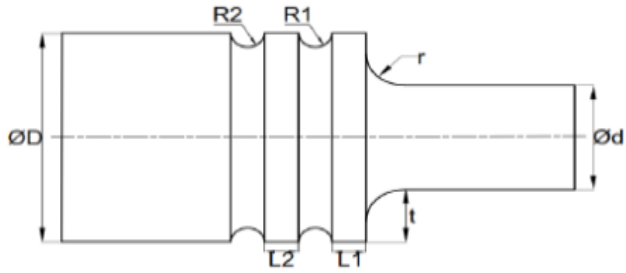

Fig. 1. Fillet addition proposed by Ali et al.

Another work was performed by Liu et al., [11], in which shaft modification was conducted by removing the end side thread and increasing the outer diameter at a certain position without changing the inner diameter, as shown in Fig. 2. Based on FEA, it is found that this optimization may reduce the stress concentration and increasethe safety factor.

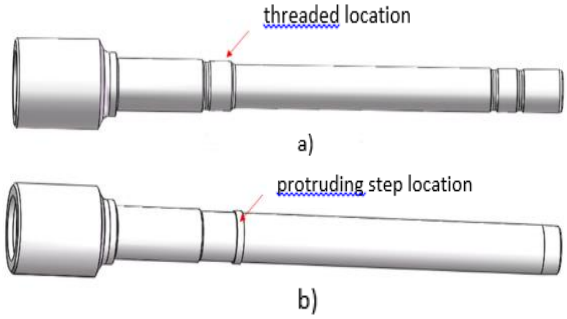

Fig. 2. Design of positive displacement motor shaft: a) initial design; b) improved design

Raychev et al [12], reported the effect of notch shape on the U-notch cylindrical specimen and specimen with shoulder fillet under axial loading. The first specimen was added a notch, which is shown in Fig. 3. The latter material used five types: U-notch, V-notch, prismatic notch, elliptical notch, and semicircular notch, as shown in Fig. 4. The results showed that U-notch outperformed in almost all variations in the two specimens proposed, indicated by the impact of max stress with eight notch types: U-notch, V-notch, prismatic notch, elliptical notch, and the double-sided notch for those mentioned.

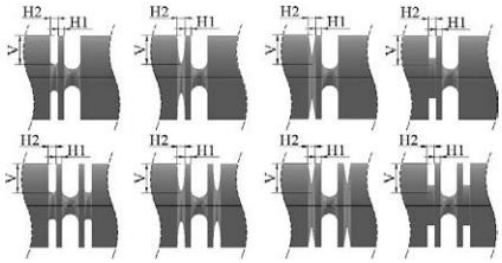

Fig. 3. Eight types of notch in U-notch cylindrical specimen

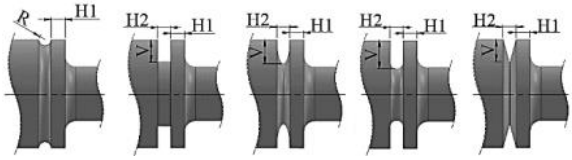

Fig. 4. Five types of notch in shoulder fillet specimen

All studies demonstrated that the modification of part dimensions of the shaft can improve the performance of the EMS. In this study, we optimized the EMS by using bearings with smaller sizes to reduce the step diameter. Subsequently followed by the investigation of the effect of step modification and tapering design in max equivalent stress and deformation which has not been yet mentioned in previous studies. This study aims to reduce shaft weight without increasing the stress concentration in the shaft. Also, we analyze the stress and deformation on the EMS by applying various load conditions.

2 Research Methods

2.1 Design input and material properties

This study adopts the design of 2 kW EMS. In which there are three (3) varied *shaft* designs will be investigated, namely, the initial EMS design, alternative 1 EMS design, and alternative 2 EMS design. The model is created using SolidWorks software. The initial shaft design is depicted in Fig. 5.

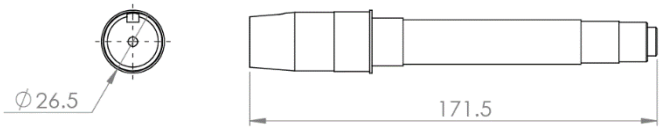

Fig. 5. Initial shaft model

There are two types of ball bearings used to support the motor shafts. The initial model used bearing type 6203 (bore diameter = 17 mm; bearing width = 12 mm). The initial bearing dimension will be replaced with the smaller size, namely bearing type 6202 (bore diameter = 15 mm; bearing width = 11 mm) and bearing type 6201 (bore diameter = 12 mm; bearing width = 10 mm). Therefore, the shaft model will be redesigned to fit the bearing size. The modified shaft design is shown in Fig. 6.

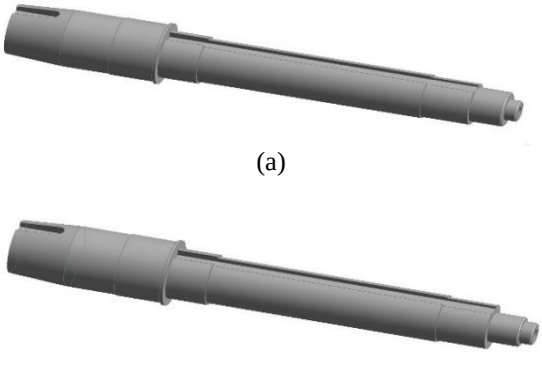

(a)

(b)

Fig. 6. Proposed shaft model: a) Alternative 1 EMS design; b) Alternative 2 EMS design

Then, the CAD model is imported into the ANSYS static structural module. The EMS material used for this simulation is AISI 1045 Steel. The mechanical properties of the EMS are presented in Table 1 [13].

Table 1. Data material properties AISI 1045 steel

Material properties	Value
Density (kg / m^3)	7870
Coefficient of Thermal Expansion (/ ^oC)	0.00000639
Reference Temperature (^oC)	20
Young's Modulus (MPa)	205.000
Poisson's Ratio (MPa)	0.29
Bulk Modulus (MPa)	162.700
Shear Modulus (MPa)	79,457
Tensile Yield Strength (MPa)	343
Compressive Yield Strength (MPa)	343
Tensile Yield Strength (MPa)	569

2.2 Mesh size setting

Meshing is a technique to divide the model into several elements. Mesh convergence is a crucial problem that needs to be addressed. This is because the quality of the finite element model depends on the quality of its mesh [14]. There are two aspects of meshing that will affect the results, namely the number and shape of elements. There is no rule of thumb to determine the perfect quantity of a mesh. Every problem must be assessed independently. However, an acceptable way to achieve satisfactory meshing is to continuously increase the density of the elements until they begin to coalesce into a single solution [15]. However, a smaller mesh size will make computations take longer time. Therefore, engineers have to make adjustments between computational accuracy and computation time [16 - 18].

To determine the optimal mesh size and type, a convergence test was performed. The applied mesh type is a tetrahedron. All designs are selected to find the most optimal mesh. In this study, the range mesh used was between 0.4 – 1.5 mm with twelve different mesh sizes for convergence test. The gap size for each successive mesh was 0.1 mm, so the mesh size used were 0.4 mm, 0.5 mm, 0.6 mm, 0.7 mm, and 0.8 mm, 0.9 mm, 1 mm, 1.1 mm, 1.2 mm, 1.3 mm, 1.4 mm, and 1.5 mm. The number of elements of each mesh size is shown in Table 2.

Table 2. Number of elements in each mesh size and bearing type

Mesh size	Number of elements		
(mm)	6203 type	6202 type	6201 type
1,5	28352	27775	26738
1,4	31678	31134	30475
1,3	37075	35181	34635
1,2	40656	39943	39470
1,1	47330	47373	46684
1	60327	58069	57890
0,9	70937	71511	70346
0,8	90820	90005	88465
0,7	121078	119400	117969
0,6	164191	164425	162524
0,5	243026	244483	241222
0,4	386542	378968	380757

All of the meshes were then analyzed with identical parameters and conditions. Solution data and the number of elements are plotted in the graph to analyze the convergence. The simulation reaches

convergence if the solution difference is below 1% between the sequential meshes [19]. The results of mesh convergence can be seen in Fig. 7.

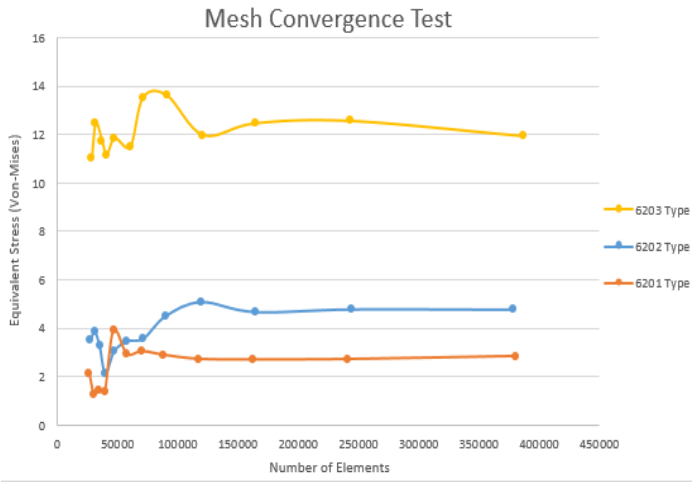

Fig. 7. Mesh convergence test result

Based on the convergence criteria, it can be concluded that the mesh with the number of elements 243,026, 244,483, and 241,222 has reached convergence. Therefore, a measure of 0.5 mm is applied to the model. The mesh generation results are depicted in Fig. 8 for all shaft models.

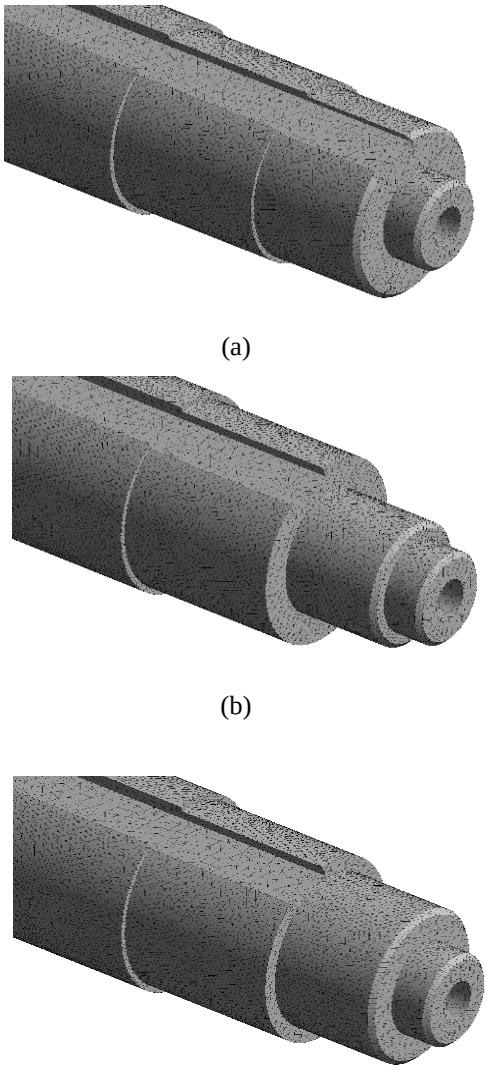

(a)

(b)

(c)

Fig. 8. Mesh generation in shaft design: a) Initial design; b) Alternative 1 design; c) Alternative 2 design

2.3 Loading configuration and solution setup

The shaft receives a bending moment due to the direct load from the pulley at one edge of the shaft and the rotor load in the middle of the shaft. Torque also occurred in the motor due to the electromagnetic force from the magnets on the rotor. Standard earth gravity and bearing weight are also considered in the calculation.

An illustration of the loading configuration is depicted in Fig. 9. The boundary conditions inserted on the shaft are the pulley load (point A), the rotor load (point B), the front bearing (point C as support and point G as the bearing load), the rear bearing (point D as support and point F as bearing load), motor torque (point E), and standard earth gravity (point H). The pulley (weight 19.2 N), rotor (28.7 N), front bearing (0.13166 N), and rear bearing (0.06356 N) are described as the force with the same direction as gravity. Torque is applied across the surface of the shaft. Standard earth gravity represents the weight of the shaft. To balance the moments and forces of these components, the front and rear bearings are used. Bearings are defined as fixed supports, which means they hold the axle shafts from moving in an axial, radial, or tangential direction.

Finally, variations in shaft design due to bearing modifications will be analyzed from the maximum equivalent stresses and deformations.

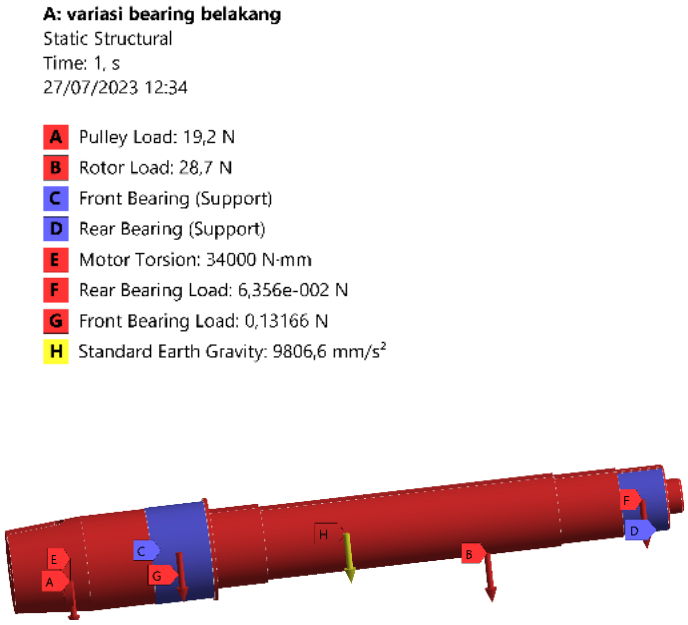

Fig. 9. Shaft Loading Configuration

3. Results and Discussion

3.1 Bearing and shaft substitution

All shaft designs have been analyzed in the static structure module to examine the influence of shaft modifications. The results of the shaft modification are depicted in Fig. 10.

The static analysis shows that the maximum equivalent stress occurs at the same area, namely the intersection of the step on the shaft, which indicates a stress concentration in that position. Another thing in this simulation is by changing the shaft step to be smaller, the maximum equivalent stress on the shaft becomes higher. The maximum equivalent stress on the 6201 bearing shaft is 54.756 MPa, which is higher than that of the existing design (30.347 MPa). Consequently, the safety factor of the modified shaft decreased.

From the deformation aspect, it can be seen that the deformation occurs in the center of the shaft. This phenomenon occurs because the greatest moment arises due to rotor load. Deformation is higher as the shaft and bearing size decrease, with the difference between the existing design and the shaft with bearing 6201 being 0,0002554 higher than the initial design.

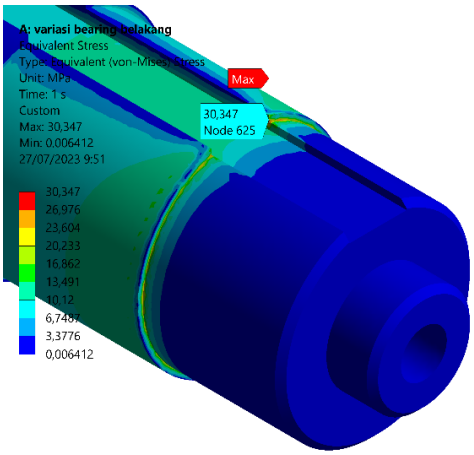

(a)

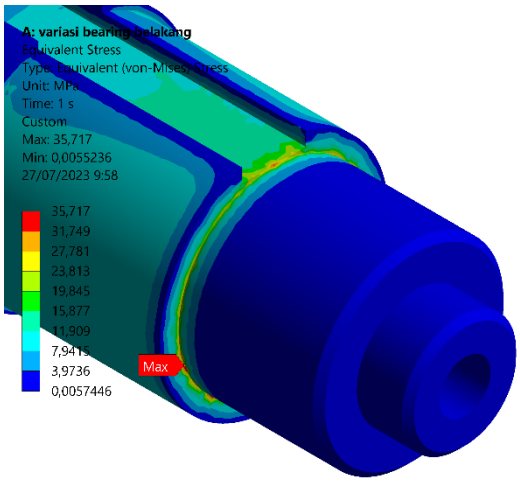

(b)

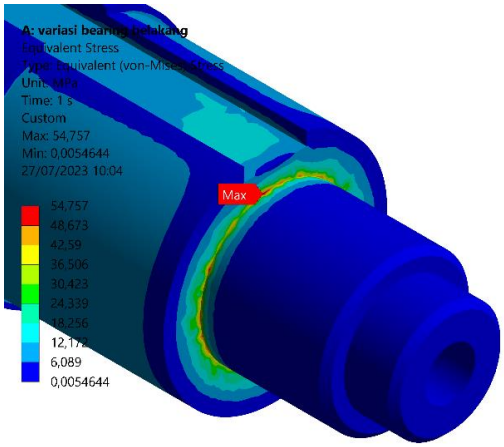

(c)

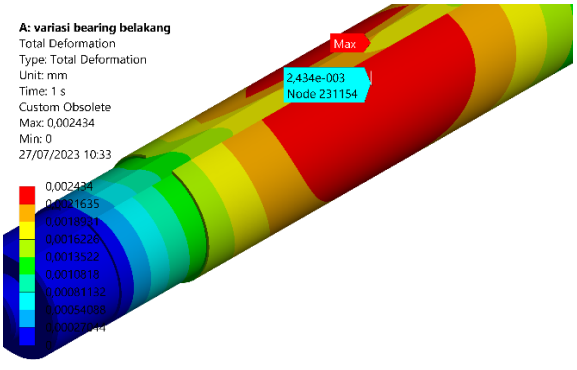

(d)

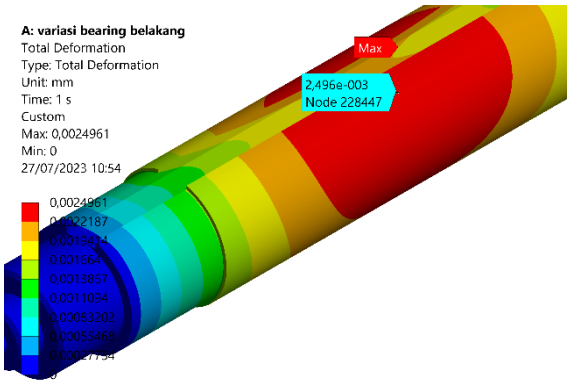

(e)

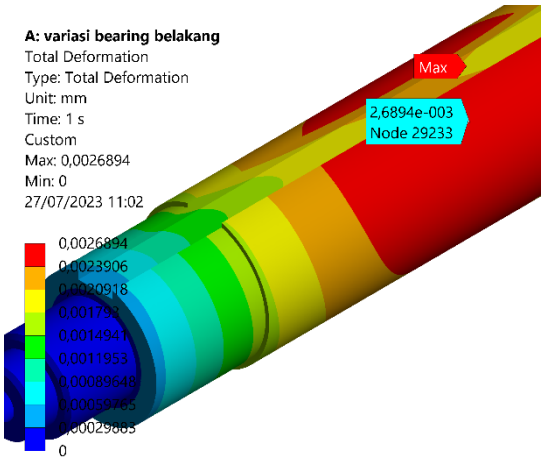

(f)

Fig. 10. Results of maximum equivalent stress deformation: a) 6203 bearing; b) 6202 bearing; c) 6201 bearing; d) deformation on 6203 bearing; e) deformation on 6202 bearing; f) deformation on 6201 bearing

A good feature of this optimization is that the shaft weight has been reduced from 431.07 g to 418.96 g. In this aspect, it can be seen that the optimization of the shaft seems to achieve success. However, this optimization carries a higher risk for the shaft. This meant that the shaft became more prone to failure, even if the optimized shaft pressure was within tolerance limits. This meant that this optimization step was partially successful.

Zhao et al [20], investigated the failure modes and the root causes of drive shaft failure in a vehicle through macroscopic and microscopic examination of fracture surface morphologies, chemical composition, metallographic analysis, and mechanical properties of materials, and theoretical finite element calculations of the drive shaft. Based on their findings, it was found that the stress concentration was one of the factors causing the failure of the drive shaft, even though the max stress (954.3 MPa) was far below the tensile yield stress (1537 MPa).

From these findings, further optimization should be carried out to reduce the stress concentration. Therefore, the next optimization method that must be performed is the modification step and tapering design.

3.2 Modification in shaft step and taper shape

To reduce stress concentration near the rear bearing mounting area, a modified shaft step was designed. The optimized design is the shaft 6201 bearings shaft because it has the lightest mass. The step modification is illustrated in Fig. 11. The notation X' remarked the diameter of the step. This parameter will be modified to find the most optimum step design. The initial diameter of the step is 17.9 mm. The step diameter is then reduced to 17.5 mm for the first iteration and further reduced continuously by 0.5 mm for each iteration. In this study, the smallest step diameter used is 12.5 mm.

Therefore, eleven iterations were carried out to find the best step design.

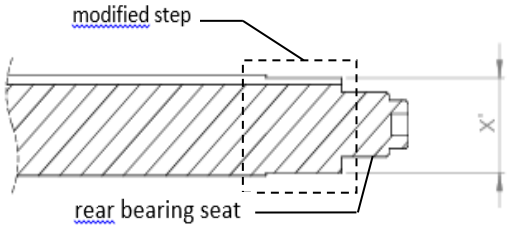

Fig. 11. The modified stepped area

The result of the second optimization is presented in Fig. 12. From this optimization, it could be concluded that the smaller the diameter of the steps, the maximum equivalent stress tends to decrease, and the deformation increases. The smallest stress value is 33.41 MPa, obtained at X' = 14 mm. At X', the shaft deformation is 0.003375078 mm. The safest value max equivalent stress is slightly higher than the existing design value. This optimization also increases the deformation value which indicates that the shaft became more flexible. In addition, there is no significant change in position at max equivalent stress and deformation.

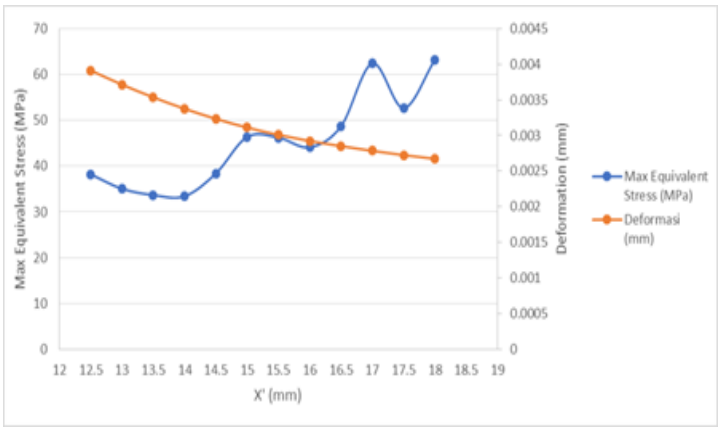

Fig. 12. The result of max equivalent stress and deformation in a variation value of X'

The next step was to create the taper. The taper is created by modifying the new step from the second optimization. Y dimension', shown in Fig. 13. The taper design was tested to check the resulting maximum equivalent stress and deformation. The biggest value of Y' is 19 mm and the smallest number is 14.5 mm. The design is iterated with a difference in the Y' value of each sequential computation of 0.5 mm.

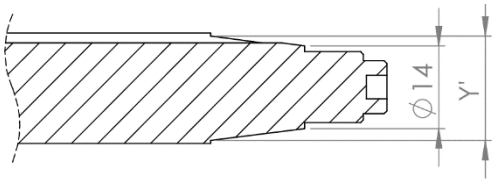

Fig. 13. The taper design

The result of the third optimization is illustrated in Fig. 14. It can be seen that from this optimization, it can be concluded that reducing Y' lowers the max equivalent stress and increases deformation. In this optimization, the taper design can help to reduce the maximum equivalent stress, even below the existing value design. The tapered design shows the most optimum result in Y' = 14.5 mm, with the max equivalent stress 28.637 MPa and deformation 0.0031063 mm. Overall, the research objective was achieved because the shaft mass and stress concentration could be reduced. The simulation summary can be seen in Table 3.

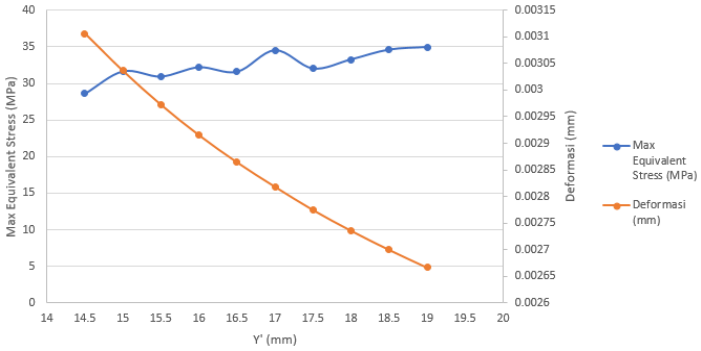

Fig. 14. The result of max equivalent stress and deformation in a variation value of X'

Table 3. Summary of the simulation result.

	Stress (MPa)	Deformation (mm)	Shaft Weight (g)
Initial	30.35	0.002434	431.07
1st optimization	54.76	0.002689	418.96
2nd optimization	33.41	0.03375	407.50
3rd optimization	28.64	0.003106	408.20

4. Conclusion

The shaft of the 2-kW induction motor has been successfully optimized by changing the rear bearing and its seat on the shaft, changing the depth of the stepped area, and creating a taper. This dimension modification was created to reduce the shaft mass and the maximum equivalent stress. At first optimization, namely changing the rear bearing and its seat on the shaft, we successfully reduced the axle weight by 2,81%. However, the max equivalent stress increased from 30.347 MPa to 54.756 MPa which is located at the intersection of the stepped area, as well as deformation also increased from 0.002434 mm to 0.0026894 mm a the center shaft. This shortcoming is overcome by changing the depth of the stepped area and creating a taper. In which the shaft mass and max equivalent stress can be reduced from 431.07 g to 408.20 g, and from 54.756 MPa to 28.637 MPa, respectively.

References

[1] S.G. Kolgiri, D.M. Sudarshan, and S.M. Nitin, "Stress Analysis for Rotor Shaft of Electric Motor", *International Journal of Application or Innovation in Engineering & Management (IJAIEM)*, Vol. 2, No. 1, pp 57-70, 2013.

[2] H.Y. Ahmad and D. Bonnieman, "Fundamental recommendations for the design configuration of rotor shafts for use in electric motors and generators", *Procedia Engineering*, Vol. 160, pp 37-44, 2016.

[3] B. Szabo and I. Babuska, "Introduction to Finite Element Analysis: Formulation, Verification and Validation", 1st Edition, West Sussex, John Wiley & Sons, Ltd, 2011.

[4] H. Patil and P. V. Jeyakarthikeyan, "Mesh convergence study and estimation of discretization error of hub in clutch disc with integration of ANSYS", *IOP Conference Series: Materials Science and Engineering*, Vol 402, pp 1-11, 2018.

[5] C. Mullen, "A Review of Finite Element Analysis with respect to Experimental Results", *16th LACCEI International Multi-*

Conference for Engineering, Education, and Technology: "Innovation in Education and Inclusion", Vol. 1, No. 1, pp 1-3, 2018.

[6] R. Prakash and Y. Mishra, "Analysis of Automobile Shaft for Optimizing Weight by Using FEM", *Smart Moves Journal Ijoscience*, Vol. 5, No. 10, pp 24-35, 2019.

[7] I.V.S. Yeswanth, A. A. E. Andrews, "Parametric Optimization of Composite Drive Shaft using ANSYS Workbench 14.0", *International Journal of Mechanical Engineering and Technology (IJMET)*, Vol. 8, No. 5, pp. 10–23, 2017.

[8] C. H. Manideep and E. Raja, "Analysis and Optimization of Composite Propeller Shaft for Automotive Applications", *International Conference on Design, Manufacturing and Materials Engineering (ICDMEE)*, Vol. 2272, No. 1, pp. 1-7, 2022.

[9] S. Saravanakumar, K. Kalaiselvan, M. Ramesh, K.B. Prakash, A. Sundar Rajan, T. Subash Chandru, M.S. Aravinth, "Design and comparison of the strength of propeller shaft for truck made of AA2024, AA7068, and Ti-6Al-4V using ANSYS", *Materials Today*, Vol. 69, No. 3, pp. 1442–1454, 2022.

[10] Ali, D. I. Permana, H. N. Yudha "Analysis of variance dimension of reinforcement to stress concentration factor using Finite Element Method", *SINERGI*, Vol. 26, No. 3, pp. 295-302, 2022.

[11] Y. Liu, Z. Lian, C. Xia, L. Qian, S. Liu, "Fracture failure analysis and research on drive shaft of positive displacement motor", *Engineering Failure Analysis*, Vol. 106, No. 7, pp. 1442–1454, 2022

[12] R. Raychev, I. Delova "Methods for Reducing the Stress Concentration in Cylindrical Specimens, at Axial Loading", *Environment. Technology. Resources*, Vol. 3, pp. 300-303. 2021.

[13] H. E. Boyer and T. L. Gall, "Metals Handbook : Desk Edition", 2nd Edition, The CRC Press, LLC, 1998.

[14] M. K. Thompson and J. M. Thompson, "ANSYS Mechanical APDL for Finite Element Analysis", 1st Edition, Oxford, Butterworth-Heinemann Elsevier, Ltd, 2017.

[15] M. Kabaluk, "Adhesive Joint Analyses Using Ansys CZM Modeling Of A Prefabricated Hybrid Concrete-GFRP-CFRP Unit", *ProQuest Dissertations And Theses*, 2019.

[16] N. S. Gukop, P. M. Kamtu, B. D. Lengs, A. Babawuya, and A. Adegoke, "Effect of Mesh Density on Finite Element Analysis Simulation of a Support Bracket", *FUOYE Journal of Engineering and Technology*, Vol. 6, No. 3, pp. 34-38, 2021.

[17] S. T. More, R. S. Bindu, "Effect of mesh size on finite element analysis of plate structure", *International Journal of Engineering Science and Innovative Technology*, Vol. 4, No. 3, pp. 181-185, 2015.

[18] A. Dutt, "Effect of mesh size on finite element analysis of beam", *International Journal of Mechanical Engineering*, Vol. 2, No. 12, pp. 8-10, 2015.

[19] C. Aliaga, K. Guan, J. Selvanayagam, J. Stokes, V. Viti, F. Menter, "Hypersonic Applications of the Laminar Turbulent Transition SST Model in ANSYS Fluent", *AIAA AVIATION Forum*, pp. 1-16, 2020.

[20] L. Zhao, Q. Xing, J. Wang, S. Li, S. Zheng, "Failure and root cause analysis of vehicle drive shaft", *Engineering Failure Analysis*, Vol. 99, pp. 225-234, 2019.